NATIONAL ADVISORY COMMITTEE FOR AERONAUTICS

TECHNICAL NOTE 2920

INTERIM REPORT ON A FATIGUE INVESTIGATION OF A FULL-SCALE TRANSPORT AIRCRAFT WING STRUCTURE

By M. James McGuigan, Jr.

Langley Aeronautical Laboratory
Langley Field, Va.

Washington
April 1953

NATIONAL ADVISORY COMMITTEE FOR AERONAUTICS

TECHNICAL NOTE 2920

INTERIM REPORT ON A FATIGUE INVESTIGATION OF A FULL-SCALE TRANSPORT AIRCRAFT WING STRUCTURE

By M. James McGuigan, Jr.

SUMMARY

Results are presented of an investigation of the fatigue strength of several full-scale aircraft wing structures. The test specimens were obtained from C-46 "Commando" type airplanes and the tests described are the first phase of a larger research program on the fatigue strength of full-scale aircraft. The tests were conducted by the resonant-frequency method at a level of 1 ± 0.625g or about 22 ± 14 percent of the design ultimate load factor.

The 34 fatigue failures which resulted from these tests were of four main types and occurred in three principal localities on the test wings. The average lifetime for these tests was about 200,000 cycles. The over-all spread for all failures was 4.4 to 1.0 and, for similar failures repeatedly occurring in the same localities, it was as low as 1.2 to 1.0. Effective stress concentration factors were calculated for all failures and indicated a value of about 4.0 for an inspection cutout and 2.3 for a riveted tension joint.

During the tests no change was noted in either the natural frequency or damping characteristics of the test specimens prior to the development of a fatigue crack. When a crack did occur, its rate of growth was rather slow until about 5 to 9 percent of the tension material had failed, after which the rate of crack growth increased rapidly.

INTRODUCTION

In recent years the problem of fatigue in aircraft structures has been accentuated by trends in aircraft design which have been detrimental to the fatigue resistance of the structures. For many years the fatigue problem has been under investigation and, for reasons of economy, the standard testing is accomplished on rather small specimens. Although this type of testing has been necessary in order to establish the basis of present-day fatigue knowledge, it does not reproduce the complex conditions which exist in a full-scale airplane structure. Therefore, some

of the results obtained by tests on small, carefully prepared specimens would not be directly applicable to a complicated aircraft structure fabricated by mass-production methods.

In view of the general lack of information regarding the fatigue characteristics of actual airplane structures, twenty-three C-46 "Commando" airplanes were secured for the purpose of carrying out a fatigue investigation on a full-scale airplane structure. The objectives of the program are to include the determination of the following: (1) the spread in fatigue life between specimens constructed in an identical manner, (2) the relative magnitude of stress concentrations caused by various types of stress raisers, (3) the effect of fatigue damage on such wing parameters as the natural frequency and the damping, (4) the reduction in static strength after fatigue failure, and (5) the loss in fatigue life associated with the flight history which an airplane has experienced. The program agreed upon was to consist of a number of constant-level tests at each of several different stress levels and a series of variable amplitude tests, based on gust-frequency data, to simulate actual flight loadings.

The present report summarizes the first phase of the program and presents the results of constant-level fatigue tests on three left and three right outer wing panels and four center wing panels. The magnitude of load for these tests was an incremental load factor of $\pm 0.625g$ about a 1 g or level-flight mean load; these load factors correspond to about 22 ± 14 percent of the design ultimate load factor. Presented in this report are the data included in reference 1, which covered the first complete wing tested, all the subsequent data collected at this test level, and a summary of all information and conclusions to date for the program. This information partially covers the first three listed objectives. The data are presented in tabular form and photographs of several fatigue cracks, spread in lifetime data, information on crack growth, experimental stress concentration factors, and comparison with some theoretical stress concentration factors are included.

SPECIMEN AND METHOD OF TEST

C-46 Structure

The C-46 wings used in these tests had previously been subjected to from 200 to 800 hours of flight service and storage for several years in

an open depot. Some geometric characteristics of the wings as well as other pertinent data for the C-46 are given in the following table:

Maximum design gross weight, lb	45,000
Level-flight equivalent airspeed, mph	240
Wing area, sq ft	1,360
Wing span, ft	108
Mean aerodynamic chord, in.	164.25
Aspect ratio	8.58
Mean thickness, percent chord	17
Design ultimate load factor	4.629

The wing structure had an all-metal, riveted, stressed-skin type of construction and was made almost entirely of 24S-T aluminum alloy. The wing consisted of three parts, a center section and two outer panels. The construction used in these panels is shown in figure 1. A truss-type rib was used in the center-panel construction, whereas a solid-sheet-type rib was used in the outer-panel construction. The outer panels were fastened to the center section by means of a heavy extruded attach angle and high-strength steel bolts. The wing skin, ribs, and most of the stiffeners were made of 24S-T alclad sheet, and the spar caps were 24S-T extrusions.

In static tests conducted by the U. S. Air Force, the wing withstood 95 percent of the ultimate design load before a failure occurred on the compression surface at span station 290. Slight changes were then made in rivet spacing in the vicinity of the failure which were considered adequate to provide the required strength. The wing was never retested subsequent to these changes. Therefore, the regions of the wing of interest to these tests are assumed capable of supporting 100 percent of ultimate design load with unknown margins of safety.

Method of Test

The method of testing selected for accomplishing these tests was the resonant-frequency method utilizing concentrated masses to reproduce the flight stresses at a selected wing station. The use of this method necessitated the selection of a station on the C-46 wing which would be critical in fatigue. Span station 214 was selected for the following reasons: (1) the wing structural analysis indicated the bending-moment margins of safety to be lowest at this station, (2) another transport aircraft in which a similar method of outer-panel attachment was utilized had experienced fatigue failures in this region of the wing, and (3) the structure at this station appeared to be of conventional design. In addition, a distributed-load static test, in which a brittle strain-indicating lacquer was used, was conducted on the wing. This test indicated that the highest strains were to be found in the neighborhood of

span station 214. Numerous points of high local stress concentration at this station were also indicated by this test. Concentrated masses, for attachment to the wing, were then proportioned and located in such a way that the 1 g bending moment, shear, and torque at span station 214 for the level-flight, low-angle-of-attack condition were reproduced.

Preparation of Wing for Test

In order to prepare the airplanes for fatigue testing, several modifications were made. The fuselage was cut off just in front of and behind the wing-fuselage attachments and the engines and landing gear were removed. The portion of the fuselage containing the wing center section was then inverted and mounted between two steel backstops. Mounting this section to the backstops was accomplished by the attachment of fabricated steel angles and steel and aluminum doubler plates which distributed the load around the fuselage.

The outer panels were cut off at a wing station 405 inches from the center line of the airplane; this reduced the span to 810 inches. The shear webs of both spars were reinforced from station 305 to station 405 to accommodate the addition of the concentrated masses at the tip. The center of gravity of these masses was located at span station 414. The specimen is shown mounted and ready for testing in figure 2.

Fatigue Machine

The constant-level fatigue machine, which also may be seen in figure 2, consisted of a prime mover, reduction gear box, line shafting, adjustable eccentric, push rod, and exciter spring. The prime mover was a direct-current traction-type electric motor, which, with the reduction gear box, was located near the center of the test setup. The motor torque was transmitted from each side of the reduction gear box by line shafting to the adjustable eccentrics which were located under the weight boxes at the wing tips. The adjustable eccentric converted the torque into a vertical force which was applied to the weight box through the push rod and spring. The spring connection was necessary in order to allow the proper phase relationship to be assumed between the wing displacement and the forcing function so that advantage could be taken of the resonant characteristics of the wing and the test could be accomplished with a minimum power input. The adjustable eccentric, push rod, and spring may be seen to the left in figure 3.

Instrumentation

The test wings were instrumented with a number of wire resistance strain gages at the points shown in figure 4. Most of these gages were

located so that the stress near the points where fatigue failures had originated on previous specimens could be measured. The gages were orientated so that the strain was measured in a spanwise direction. The validity of this orientation was checked in most locations by the use of a rosette type of strain-gage configuration in order to determine the direction of the principal stress. The diamond-shaped symbols in figure 4 denote the location of gages which were used continuously to measure directly the applied bending moments.

Fatigue-crack-detector wires were used to indicate the presence of fatigue failures. They consisted of fine, insulated copper wire cemented to the structure in such a manner that the wire would break when a crack passed under it. These wires were capable of detecting a crack as small as 0.0002 inch in width. A break in the wire actuated an indicator system on the control table. The locations of these wires are also shown in figure 4. These locations were determined in the brittle-lacquer test previously referred to and by the occurrence of cracks in previous specimens.

In order to obtain a count of the loads applied during the tests, a system of mechanically operated microswitches, which may be seen to the right in figure 3, were used to actuate a bank of counters. These counters indicated the number of times the amplitude of vibration of the wing exceeded a predetermined magnitude.

The frequency of vibration was maintained by an electronic speed control and was indicated by a stroboscopic tachometer. This sensitive motor-speed-control and indicating system was necessary because the wings were vibrated exactly at their resonant frequency, and even very small variations in the frequency of the forcing function would cause the amplitude of vibration to drop excessively because of the low damping of the structure.

TESTS AND PROCEDURE

The tests were carried out by vibrating the wings at a constant amplitude at their resonant frequency of 108 cycles per minute with the fatigue machine previously mentioned. The amplitude of vibration for the specimens covered in this paper was $\pm 0.625g$ about the 1 g mean given by the concentrated masses attached to the wing. This load was selected for these first tests in order to insure a reasonable testing time. A comparison of the 1 g design bending moment for this wing and the bending moment applied by the concentrated masses is shown in figure 5. This figure indicates that the applied bending moment without nacelle inertia effects reproduced rather closely the design bending moment not only at station 214 but over a considerable portion of the span from about station 300 inboard. As a result of this close simulation and because

of the uniformity of design, failures could be expected to occur anywhere over this whole region. With the addition of the nacelle inertia effects, the bending moment is reduced slightly from station 178 inboard. The tests were started without the nacelle effects, but, since failures occurred in the center section, this load was added to reduce the stress inboard of that point and to made certain that failure would occur in the outer panels.

Continuous visual inspection throughout the tests supplemented any indications from the fatigue-crack-detector wires. These visual inspections were made while the wing was vibrating in an effort to reduce stopping and starting to a minimum and thus eliminate many cycles of load at other than the desired level. At various times throughout the tests, the response of all strain gages was recorded and checked for consistency of loading.

The testing of a specimen was continued until a fatigue failure occurred and, if the failure occurred in the center section, it was usually repaired in order to continue testing the outer panels. When failures appeared in the outer panels they were allowed to grow and their rate and manner of propagation was noted.

RESULTS AND DISCUSSION

Definition of Fatigue Failure

In tests conducted on small specimens, the number of cycles to failure is usually taken at the time of complete severing of the test specimen. However, for tests conducted on as large a structure as a complete aircraft wing, this definition is not very practical, since in a structure of this size a great many cycles can elapse between the inception of a fatigue crack and the failure of the complete wing. During this time, the growing crack and the impending failure are perfectly obvious. In addition, any visible crack discovered in an actual aircraft structure is usually cause for repair or replacement. Therefore, for purposes of this investigation, a fatigue failure is defined as a break in the material of the wing that is approximately 1/4 inch long and as deep as the thickness of the material in which it originated. A few of the failures which are reported in this paper were not discovered until they had exceeded this length. However, the number of cycles to cause failure was corrected to this common basis. This correction was based on the assumption of a uniform rate of crack growth and on indications of change in the natural frequency of the test specimen caused by the growing fatigue crack.

Load History of Specimens

The load histories for each of the 34 fatigue failures which occurred in these specimens are listed in a summation form in table 1. For purposes of identification, the cracks are numbered in order of their occurrence. The columns listed under the summation of load cycles equal to or greater than Δn threshold values are the cycles counted directly by the bank of counters used in the tests and Δn is the incremental load factor. These counters counted the number of cycles which equaled or exceeded their assigned amplitude and thus gave the load histories in a summation form. The columns listed under the number of load cycles applied in a class interval are the cycles which acted only at levels between the threshold values defining that class interval. For failure 1, for instance, 14,456 cycles (295,089 - 280,633) are assumed to act at a Δn value of 0.225 which is the mean of $\Delta n = 0.15$ and $\Delta n = 0.30$. Cycles applied in other class intervals are also assumed to act at the midpoint of their interval with the exception of the interval between $\Delta n = 0.60$ and $\Delta n = 0.75$. These loads are assumed to act at $\Delta n = 0.625$ since this value was the desired load level and every effort was made to maintain it. The average lifetime at this desired level was about 200,000 cycles.

Although the tests were intended to be of the constant-level type at a load-factor increment of 1 ± 0.625, some few cycles at other load levels were applied. This fact can readily be seen in table 1; these cycles, in general, were imposed during preliminary surveys or while the machine was building up to or dying down from the desired level. The average number of these departures from the constant level is shown in figure 6 in which the average number of cycles applied in each class interval is shown graphically.

Description of Fatigue Failures

The fatigue failures that occurred in the specimens tested appeared to be concentrated in three principal localities. One locality was in the vicinity of the station designated as critical - span station 214 on the outer panel - in which 15, or almost half, of the failures took place. Another locality was in the vicinity of the engine nacelle where 12 failures appeared, and the third locality was a region in the center section of the wing near the center line of the aircraft where 7 failures appeared.

The fatigue failures that occurred were divided into the following four main types according to the type of structural-stress raiser in which they initiated:

Type I	Corner of inspection cutout
Type II	Riveted tension joint
Type III	Riveted shear joint
Type IV	Discontinuities in section or shape

The first type included the 10 failures which originated at the corners of inspection cutouts. The second type included the 6 failures which occurred in a riveted tension joint near the center line of the aircraft. The third type included the 6 failures which occurred in a riveted shear joint where the shear web of the front spar was riveted to the tension flange of that spar. The fourth type included 12 failures which originated at abrupt changes or discontinuities in section or shape, such as the edge of a reinforcing doubler plate. The points of initiation for these four types of failure are shown in figure 7 which is a plan view of the tension surface of the wing. For convenience, failures that occurred on both wings are shown on a portion of one semispan.

The failures of type I, which occurred at the corners of inspection cutouts, all originated on the outer panels in the vicinity of span station 214. The chordwise distribution of stress through this section, as measured with strain gages, is shown in figure 8. Failure 3, which is a typical example of this type of failure, is shown in figure 9(a) a short time after starting and again in figure 9(b) after it had progressed to a length of about 17 inches. In figure 9(c) the same crack is shown after causing failure of the spar at the 30-percent-chord position. Another failure of this type is shown in figure 10. The crack originated at the cutout nearest the rear spar at span station 214 and was repeated more often than any other failure of this type. It appeared on all three left wings and on the third right wing. In no case, however, did this crack result in final failure of the wing. The failures originating in this identical location were failures 5, 17, and 33 on the left wing and 26 on the right wing. Failures occurring at the same locations on the left and right wings will be considered as identical for purposes of further discussion.

The details of construction in the vicinity of all the cutouts on the outer panels were somewhat similar. The cutouts were all located between two spanwise stiffeners, which were adjacent to the edges of the cutouts, and were also reinforced by doubler plates underneath the wing skin. These doubler plates were about $1\frac{3}{4}$ times as long, spanwise, as the cutouts and extended chordwise underneath the stiffener on each side.

Although the corners of most of the inspection cutouts have fairly large radii, the corners of some of the reinforcing doubler plates underneath the cutouts have much smaller radii. This situation caused the initiation of some failures in the doubler plates which in one case progressed into the wing skin. An example of the start of one of these failures is shown in figure 11.

The second type of failure occurred in a riveted tension joint 32 inches from the aircraft center line. The joint extended chordwise at this wing station from the front spar to the rear spar. Failures of this type appeared on the left and right wing of the first three wing center sections in the same chordwise location and are listed as failures 1, 2, 11, 14, 22, and 23. The details of this joint and the manner of failure are shown in figure 12. The measured chordwise stress distribution through this section is shown in figure 13, from which it may be seen that the highest stress occurs at the point where all the failures originated.

The third type of failure occurred in a riveted shear joint at span station 120 where the shear web of the front spar was riveted to the tension flange of that spar. There were four horizontal rows of rivets in the shear web and the fatigue failures originated in a rivet in the third row away from the tension surface of the wing as can be seen in figure 14. These failures are numbered 8, 9, 20, 21, 28, and 32. Although this joint is designed primarily for shear, strain-gage rosette measurements near the point of failure showed the principal stress to be approximately parallel to the tension flange of the spar. This condition would indicate that the failures were probably primarily due to tension stresses. The shear at this point in the spar was probably small since the spar ends a short distance outboard of this point as can be seen in figure 7.

A typical example of those cracks which occurred at the junction of the engine nacelle and the wing spar and which are grouped in the fourth type is shown in figure 15. The failure shown is similar to failures 6, 7, 18, 19, and 30 and originated in a rivet hole near a half-round notch cut in the edge of the skin to eliminate interference of the landing-gear retracting strut with the wing skin during operation of the landing gear. Another failure of the fourth type which was repeated often occurred in a chordwise joggle in an external doubler plate near the wing attach angle. These failures appeared in three left wings and one right and are numbered 4, 10, 16, and 29. Failures were expected to occur at this point since the brittle-lacquer static test had indicated a high stress in this region. An example of this failure is shown in figure 16 after it had progressed to a considerable length.

Only one of the failures that occurred (failure 24) originated in the wing spar flanges, and it was of the fourth type. This failure occurred in the front-spar tension flange 11 inches from the aircraft center line and originated at a hole in the flange to which a non-load-carrying bracket had been bolted.

Spread in Fatigue Life

The over-all spread in number of cycles to failure for all 34 of the failures that occurred was 4.4 to 1.0. This spread is comparable to that obtained in small specimen tests, but, when the spread for each of the four types of fatigue failures is examined individually, a lower value is obtained for most types. It should be realized, however, that the number of failures in each type is rather small for spread determination.

For the 10 type I failures, that is, those occurring at the corners of inspection cutouts, the total spread is 1.54 to 1.0; however, for failures 5, 17, 26, and 33, all of which originated at the same location in the structure, the spread is only 1.2 to 1.0. For the 6 type II failures, which were those failures occurring in the riveted tension joint, the spread was 2.17 to 1.0. The spread for the 6 type III failures, at the riveted shear joint, was 1.83 to 1.0. The 12 type IV failures had a spread of 4.4 to 1.0 which accounts for the larger over-all range. This wider range is explained in part by the variety of stress raisers which were included in this classification.

In general, the spread for similar failures is somewhat smaller than that expected of tests run on simple specimens.

Stress Concentration Factors

Since the measurement of the true maximum stress caused by a stress raiser is very difficult, no attempt was made during these tests to make such a measurement. Instead, only the nominal stress in the vicinity of the stress raiser was measured and any effects from the stress raiser were purposely excluded. The effective stress concentration factor or fatigue-strength reduction factor was then deduced from the data by two methods. In order to utilize these two methods, the measured mean and maximum stresses present during a loading cycle are required; these values are listed in the fourth and fifth columns of table 2 for each failure. A small correction was made in a few of these stresses for the failures inboard of span station 178 in which the stress was affected somewhat by the introduction of the nacelle inertia effects.

The calculation of the effective stress concentration factor for a constant-level test with zero mean stress could be accomplished by first determining an effective maximum local stress, caused by the stress raiser, which must have been present in order for a failure to occur at the number of cycles noted in the test. This effective stress is found from the S-N curve for the plain material without stress raisers and is divided by the measured stress to determine the stress concentration factor.

The first method of calculating a stress concentration factor for these tests followed a method similar to that outlined in the preceding paragraph. It was complicated, however, by the presence of the 1 g mean stress caused by the concentrated masses attached to the wing and by the frequency distribution shown in figure 6. In order to pursue this method of analysis, all the fatigue damage was assumed to be caused only by the number of loads applied in the class interval from $\Delta n = 0.60$ to $\Delta n = 0.75$ and, furthermore, all these loads were assumed to have acted at a Δn value of 0.625, the desired level. The effective stress concentration factor K_1 was then defined as

$$K_1 = \frac{\sigma_{S-N}}{\sigma_{max}}$$

In this expression, σ_{max} is the measured stress at a load factor of 1.625 (table 2, fifth column) and σ_{S-N} is that effective maximum stress, mentioned previously, that must have been present in order for a failure to occur at the number of cycles noted in the test (table 2, seventh column). The effective stress was determined, in this case, from the S-N curve that can be drawn for a mean stress of σ_{mean} (the measured 1 g mean stress) times K_1. In other words, the concentration factor was applied to both the mean and the maximum measured stress present in a loading cycle. The quantities K_1 and σ_{S-N} were therefore interdependent. In order to determine the value of K_1 for each failure, a trial-and-error method was employed wherein different values were assigned to K_1 until a value of σ_{S-N} was found which was equal to σ_{max} times K_1. This condition is necessary in order to satisfy the defining equation for K_1. The S-N curves used to determine σ_{S-N} were based on data for 0.040-inch-thick unnotched 24S-T alclad sheet as given in reference 2. The values of σ_{S-N} and K_1 thus determined are listed in the seventh and eighth columns of table 2. This method is the equivalent of dividing the maximum stress during a loading cycle for an unnotched specimen by the maximum nominal stress for a notched specimen at the same load ratio and lifetime.

Since the amplitude of the applied stress cycles was not exactly at a constant level during these tests, the fatigue-damage theory described in reference 3 was also used to compute an effective stress concentration factor K_2. This theory indicates that failure will occur when the summation curve of the loading cycles becomes tangent to the S-N curve. The determination of the effective stress concentration factor by this theory is illustrated in figure 17 for one of the fatigue failures. Data on unnotched 0.040-inch 24S-T alclad sheet reported in reference 2 were also used to plot the S-N curves shown in this figure. The solid lines in figure 17 show the S-N curves for the pertinent mean stress values. The dashed lines represent the summation curves or the number of loads applied equal to or greater than the stresses corresponding to the Δn threshold values. The lower dashed line represents measured stress values whereas

the upper dashed line represents the measured stress values moved vertically until they become tangent to the S-N curve having the proper mean stress value. This adjustment, in effect, was accomplished by multiplying the measured stress values by a constant K_2 which, in a similar manner to K_1, is the effective stress concentration factor. The K_2 factors calculated by this method are listed in the ninth column of table 2 and differ only slightly from those found by the first method.

Association of the K values from table 2 with the four different types of failures shows that, for the 10 type I failures originating at the corners of inspection cutouts, the effective stress concentration factors varied from 3.73 to 4.60 by both methods of calculation. The mean value for this type of failures was 4.14. The effective stress concentration factors for the 6 type II failures occurring in the riveted joint at span station 32 varied only from 2.17 to 2.55. The mean value for this type of failure was 2.30. These factors were based on the net area stress in the joint. Concentration factors calculated for the third type of failure, the riveted shear joint, varied from 2.92 to 3.67 and were based on the normal stress. For the fourth type of failure the factors calculated varied from 2.6 to 5.2. The highest factor calculated was for a failure in a joggle discontinuity in an external doubler plate. The larger spread in concentration factors calculated for the fourth type of failure is due to the variety of structural stress raisers included in that classification.

The only type of failure encountered which lends itself to a theoretical treatment is the type I failure occurring at the inspection cutout. In reference 4 a theoretical concentration factor has been derived for a "square" cutout with a corner radius proportional to its width. By utilizing this factor and making a correction for the actual corner radius of the cutouts in question, theoretical stress concentration factors were calculated for all six of the cutouts where fatigue failures had occurred. These theoretical factors varied from 3.0 to 4.8 for the various cutouts compared to the experimental factors of 3.7 to 4.6. In almost all cases the theoretical factor was less than the experimental factor.

Rate of Crack Growth

Several of the fatigue cracks in the wing outer panels were allowed to grow until a considerable amount of the tension surface had failed. The rate at which the cracks grew is shown in figure 18, in which the percent of cross-sectional material failed in the tension surface at the wing station where the failure occurred is plotted as a function of the number of cycles of load applied. The crack-growth curves of figure 18 indicate that the propagation of the cracks was relatively slow until about 5 to 9 percent of the tension material had failed. At this point the slopes of the curves abruptly become very steep and thereby indicate a rapid propagation of the crack thereafter. The abrupt discontinuity in

one of the curves (failure 31) was caused by the sudden failure of a large stiffener. In spite of this, the curve exhibits the same rapid increase in rate of crack growth between 5 and 9 percent failure of the tension material. It must be recognized, however, that this slow initial rate of crack growth does not preclude the possibility of a failure initiating undetected in a large stiffener or spar flange which in itself has a larger percentage of tension area than the 5 to 9 percent value mentioned. It is also probable that this percentage might depend to some extent on the stress level at the crack.

Effect of Fatigue Damage on Natural Frequency and Damping

The tests indicated that the natural frequency of the test wings was not affected by fatigue damage until after a fatigue failure had originated. Even then, the change in natural frequency was very small and amounted to only about 2.0 percent with as much as 55 percent of the tension material failed in fatigue. In figure 19 the indicated change in natural frequency is plotted as a function of percent of tension material failed for several of the failures.

Since the tests were conducted at the resonant frequency of the test specimens, any change in damping characteristics would cause a corresponding change in the amplitude of vibration. As no such change in amplitude was noted during the course of the tests, it can be concluded that fatigue damage has little or no effect on the structural damping characteristics of a full-scale aircraft wing.

Measurements of the natural frequency or structural damping characteristics of an airplane wing would, therefore, appear to be of no practical value as an indication of incipient fatigue failure.

CONCLUDING REMARKS

Constant-level fatigue tests conducted on several full-scale C-46 "Commando" airplane wings at a level of $1 \pm 0.625g$ indicated a lifetime at this level of about 200,000 cycles. The 34 fatigue failures which resulted from these tests were of four main types and occurred in three principal localities on the wing. The spread in fatigue life for the structure was comparable to the spread for the material. For all failures the spread was 4.4 to 1.0, and failures repeatedly occurring at the same locations exhibited spreads as small as 1.2 to 1.0. Effective stress concentration factors were calculated for all failures and indicated a value of about 4.0 for an inspection cutout and 2.3 for a riveted tension joint.

During the tests no change was noted in either the natural frequency or structural damping characteristics of the test specimens prior to the development of a fatigue crack. When a crack did occur, its rate of growth was rather slow until about 5 to 9 percent of the tension material had failed, after which the rate of crack growth increased rapidly.

Langley Aeronautical Laboratory,
National Advisory Committee for Aeronautics,
Langley Field, Va., January 8, 1953.

REFERENCES

1. Fearnow, Dwight O.: Investigation of the Fatigue Strength of Full-Scale Airplane Wing Structures. NACA RM L51D13a, 1951.

2. Russell, H. W., Jackson, L. R., Grover, H. J., and Beaver, W. W.: Fatigue Strength and Related Characteristics of Aircraft Joints. II - Fatigue Characteristics of Sheet and Riveted Joints of 0.040-Inch 24S-T, 75S-T, and R303-T275 Aluminum Alloys. NACA TN 1485, 1948.

3. Bland, Reginald B., and Sandorff, Paul E.: The Control of Life Expectancy in Airplane Structures. Aero. Eng. Rev., vol. 2, no. 8, Aug. 1943, pp. 7-21.

4. Greenspan, Martin: Effect of a Small Hole on the Stresses in a Uniformly Loaded Plate. Quarterly Appl. Math., vol. II, no. 1, Apr. 1944, pp. 60-71.

TABLE 1

LOAD HISTORY FOR ALL FATIGUE FAILURES

Failure (a)	Summation of load cycles equal to or greater than Δn threshold values of -												
	0.15		0.30		0.45		0.60		0.75		0.90		1.05
	Number of load cycles applied in class interval, assumed acting at Δn values of -												
		0.225		0.375		0.525		0.625		0.825		0.975	
1	295,089	14,456	280,633	29,787	250,846	71,814	179,032	170,632	8,400	8,262	138	118	14
2	332,542	16,866	315,676	31,823	283,853	79,919	203,934	195,534	8,400	8,262	138	118	14
3	332,542	16,866	315,676	31,823	283,853	79,919	203,934	195,534	8,400	8,262	138	118	14
4	353,898	17,473	336,425	35,028	301,397	88,549	212,848	204,448	8,400	8,262	138	118	14
5	448,095	19,686	428,409	37,010	391,399	98,335	293,064	282,701	10,363	10,225	138	118	14
6	224,470	6,309	218,161	9,983	208,178	29,342	178,836	171,371	7,465	7,465	0	0	0
7	224,470	6,309	218,161	9,983	208,178	29,342	178,836	171,371	7,465	7,465	0	0	0
8	224,470	6,309	218,161	9,983	208,178	29,342	178,836	171,371	7,465	7,465	0	0	0
9	224,470	6,309	218,161	9,983	208,178	29,342	178,836	171,371	7,465	7,465	0	0	0
10	333,631	8,930	324,701	10,899	313,802	31,789	282,013	274,369	7,644	7,644	0	0	0
11 (1)	371,524	9,595	361,929	11,724	350,205	34,282	315,923	308,279	7,644	7,644	0	0	0
12	264,378	6,991	257,387	6,936	250,451	17,747	232,704	227,023	5,681	5,681	0	0	0
13	413,199	11,445	401,754	13,222	388,532	38,224	350,308	342,664	7,644	7,644	0	0	0
14 (2)	427,078	11,508	415,570	13,381	402,189	39,474	362,715	355,071	7,644	7,644	0	0	0
15	246,376	9,190	237,226	8,780	228,446	22,763	205,683	205,504	179	179	0	0	0
16 (4)	283,159	10,185	272,974	9,786	263,188	24,563	238,625	238,446	179	179	0	0	0
17 (5)	297,454	10,351	287,103	9,958	277,145	25,167	251,978	251,799	179	179	0	0	0

[a] Numbers in parentheses indicate repetitions of previous failures.

TABLE 1.- Concluded

LOAD HISTORY FOR ALL FATIGUE FAILURES

Failure (a)	Summation of load cycles equal to or greater than Δn threshold values of -												
	0.15		0.30		0.45		0.60		0.75		0.90		1.05
	Number of load cycles applied in class interval, assumed acting at Δn values of -												
		0.225		0.375		0.525		0.625		0.825		0.975	
18 (7)	106,328	5,495	100,833	7,036	93,797	15,677	78,120	78,120	0	0	0	0	0
19 (6)	149,951	5,727	144,224	7,293	136,931	17,198	119,733	119,733	0	0	0	0	0
20 (8)	174,727	5,996	168,731	7,528	161,203	18,033	143,170	143,170	0	0	0	0	0
21 (9)	174,727	5,996	168,731	7,528	161,203	18,033	143,170	143,170	0	0	0	0	0
22 (2, 14)	198,574	6,723	191,851	7,831	184,020	19,248	164,772	164,463	309	309	0	0	0
23 (1, 11)	198,574	6,723	191,851	7,831	184,020	19,248	164,772	164,463	309	309	0	0	0
24	263,956	10,814	253,142	10,382	242,760	23,590	219,170	217,096	2,074	2,074	0	0	0
25	299,657	11,641	288,016	11,966	276,050	28,731	247,319	245,245	2,074	2,074	0	0	0
26	299,657	11,641	288,016	11,966	276,050	28,731	247,319	245,245	2,074	2,074	0	0	0
27	251,111	6,428	244,683	5,286	239,397	17,251	222,146	220,072	2,074	2,074	0	0	0
28 (8, 20)	106,397	1,166	105,231	1,990	103,241	9,529	93,712	93,712	0	0	0	0	0
29	396,686	12,239	384,447	12,686	371,761	35,089	336,672	334,598	2,074	2,074	0	0	0
30 (7, 18)	132,065	1,522	130,543	2,324	128,219	10,678	117,541	117,541	0	0	0	0	0
31	303,487	6,990	296,497	5,847	290,650	20,173	270,477	268,403	2,074	2,074	0	0	0
32 (9, 21)	171,969	2,091	169,878	2,903	166,975	14,325	152,650	152,650	0	0	0	0	0
33 (5, 17)	336,583	7,512	329,071	6,346	322,725	22,650	300,075	298,001	2,074	2,074	0	0	0
34	340,051	7,512	332,539	6,346	326,193	22,650	303,543	301,469	2,074	2,074	0	0	0

a Numbers in parentheses indicate repetitions of previous failures.

TABLE 2

SUMMARY OF DATA

Failure (a)	Location of failure (b)	Type of failure	Measured stress		Applied loads at $\Delta n = 0.625$, cycles	Stress from S-N curve, σ_{S-N}, psi	K_1	K_2
			1 g σ_{mean}, psi	1.625g σ_{max}, psi				
1	Riveted tension joint, station 32 (L, CS, 1)	II	11,263	18,303	170,632	41,548	2.27	2.30
2	Riveted tension joint, station 32 (R, CS, 1)	II	11,212	18,219	195,534	39,535	2.17	2.25
3	Corner of inspection cutout, station 214 (R, OP, 1)	I	6,574	10,683	195,534	39,848	3.73	3.80
4	Joggle in external doubler plate, station 195 (L, OP, 1)	IV	4,849	7,880	204,448	38,848	4.93	5.20
5	Corner of inspection cutout, station 214 (L, OP, 1)	I	5,210	8,466	282,701	36,827	4.35	4.47
6	Outboard juncture of wing and nacelle, station 180 (R, CS, 2)	IV	6,965	11,318	171,371	41,537	3.67	3.73
7	Outboard juncture of wing and nacelle, station 180 (L, CS, 2)	IV	7,187	11,679	171,371	41,460	3.55	3.63
8	Riveted shear joint, station 120 (R, CS, 2)	III	8,801	14,302	171,371	41,762	2.92	2.98
9	Riveted shear joint, station 120 (L, CS, 2)	III	8,801	14,302	171,371	41,762	2.92	2.98
10	Joggle in external doubler plate, station 189 (L, CS, 2)	IV	4,751	7,720	274,369	37,056	4.80	5.00
11 (1)	Riveted tension joint, station 32 (L, CS, 2)	II	10,134	16,470	308,279	36,234	2.20	2.27
12	Edge of external doubler plate, station 207 (R, OP, 2)	IV	9,104	14,794	227,023	38,464	2.60	2.68
13	Inboard juncture of wing and nacelle, station 135 (L, CS, 2)	IV	6,130	9,961	342,664	35,660	3.58	3.67
14 (2)	Riveted tension joint, station 32 (R, CS, 2)	II	9,955	16,177	355,071	35,589	2.20	2.25
15	Corner of inspection cutout, station 214 (L, OP, 2)	I	6,158	10,007	205,504	39,027	3.90	4.10
16 (4)	Joggle in external doubler plate, station 195 (L, OP, 2)	IV	4,848	7,880	238,446	38,139	4.84	5.00
17 (5)	Corner of inspection cutout, station 214 (L, OP, 2)	I	5,210	8,466	251,799	38,097	4.50	4.58

[a]Numbers in parentheses indicate repetitions of previous failures.

[b]Letters in parentheses refer to the following: L, left wing; R, right wing; CS, center section; OP, outer panel. Numbers in parentheses refer to the order in which wing sections were tested.

TABLE 2 - Concluded

SUMMARY OF DATA

Failure (a)	Location of failure (b)	Type of failure	Measured stress		Applied loads at $\Delta n = 0.625$, cycles	Stress from S-N curve, σ_{S-N}, psi	K_1	K_2
			1 g σ_{mean}, psi	1.625g σ_{max}, psi				
18 (7)	Outboard juncture of wing and nacelle, station 180 (L, CS, 3)	IV	7,187	11,679	78,120	50,220	4.30	4.50
19 (6)	Outboard juncture of wing and nacelle, station 180 (R, CS, 3)	IV	6,965	11,318	119,733	45,159	3.99	4.20
20 (8)	Riveted shear joint, station 120 (R, CS, 3)	III	8,585	13,950	143,170	43,318	3.12	3.24
21 (9)	Riveted shear joint, station 120 (L, CS, 3)	III	8,585	13,950	143,170	43,245	3.10	3.20
22 (2, 14)	Riveted tension joint, station 32 (R, CS, 3)	II	10,950	17,794	164,463	41,816	2.35	2.43
23 (1, 11)	Riveted tension joint, station 32 (L, CS, 3)	II	10,914	17,734	164,463	42,030	2.37	2.55
24	Front spar tension flange, station 11 (L, CS, 3)	IV	7,725	12,553	217,096	38,914	3.10	3.20
25	Corner of inspection cutout, station 228 (R, OP, 3)	I	6,260	10,173	245,245	38,047	3.74	3.80
26	Corner of inspection cutout, station 214 (R, OP, 3)	I	5,210	8,466	245,245	38,097	4.50	4.60
27	Corner of inspection cutout, station 239 (L, OP, 3)	I	6,004	9,757	220,072	38,833	3.98	4.10
28 (8, 20)	Riveted shear joint, station 120 (R, CS, 4)	III	8,330	13,536	93,712	48,188	3.56	3.67
29	Joggle in external doubler plate, station 195 (R, OP, 3)	IV	4,736	7,696	334,598	35,709	4.64	4.78
30 (7, 18)	Outboard juncture of wing and nacelle, station 180 (L, CS, 4)	IV	7,187	11,679	117,541	45,548	3.90	4.03
31	Corner of inspection cutout, station 214 (L, OP, 3)	I	6,158	10,007	268,403	37,426	3.74	3.84
32 (9, 21)	Riveted shear joint, station 120 (L, CS, 4)	III	8,330	13,536	152,650	42,503	3.14	3.26
33 (5, 17)	Corner of inspection cutout, station 214 (L, OP, 3)	I	5,210	8,466	298,000	36,404	4.30	4.47
34	Corner of inspection cutout, station 206 (L, OP, 3)	I	5,532	8,990	301,469	36,679	4.08	4.18

[a]Numbers in parentheses indicate repetitions of previous failures.

[b]Letters in parentheses refer to the following: L, left wing; R, right wing; CS, center section; OP, outer panel. Numbers in parentheses refer to the order in which wing sections were tested.

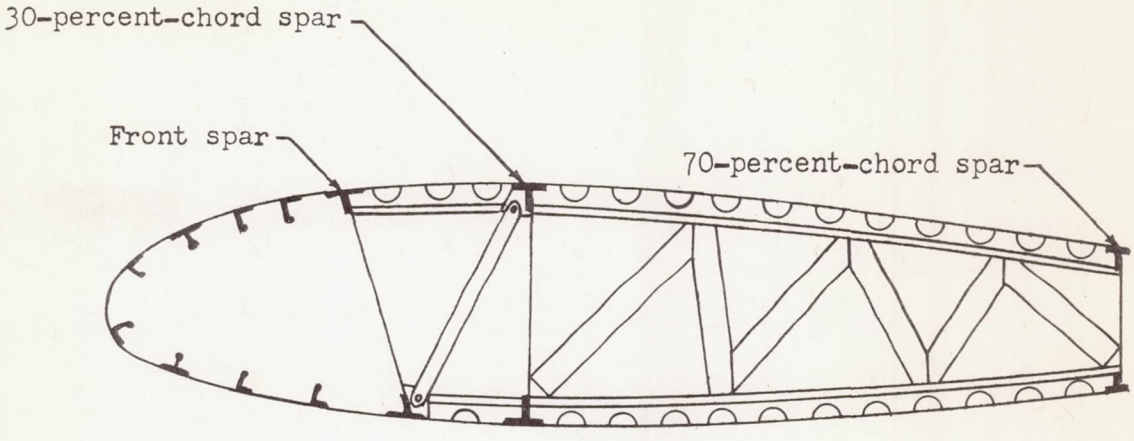

Center-panel structure

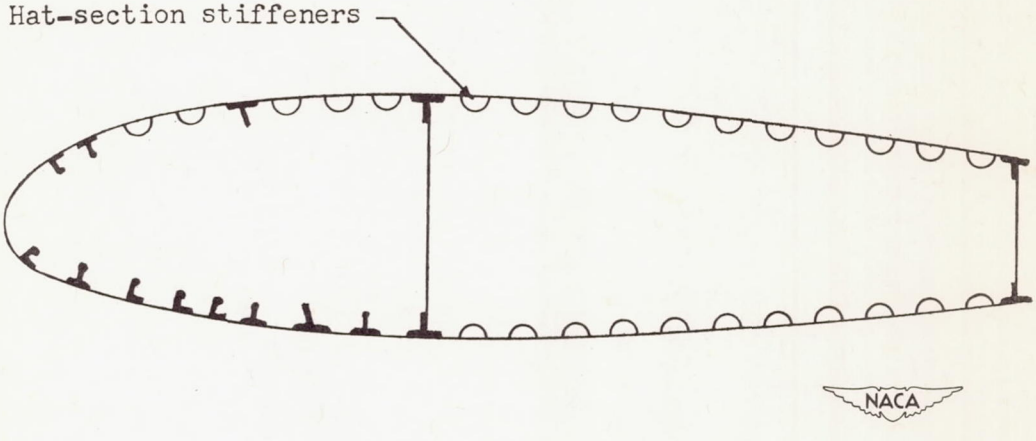

Outer-panel structure

Figure 1.- Typical cross section of wing.

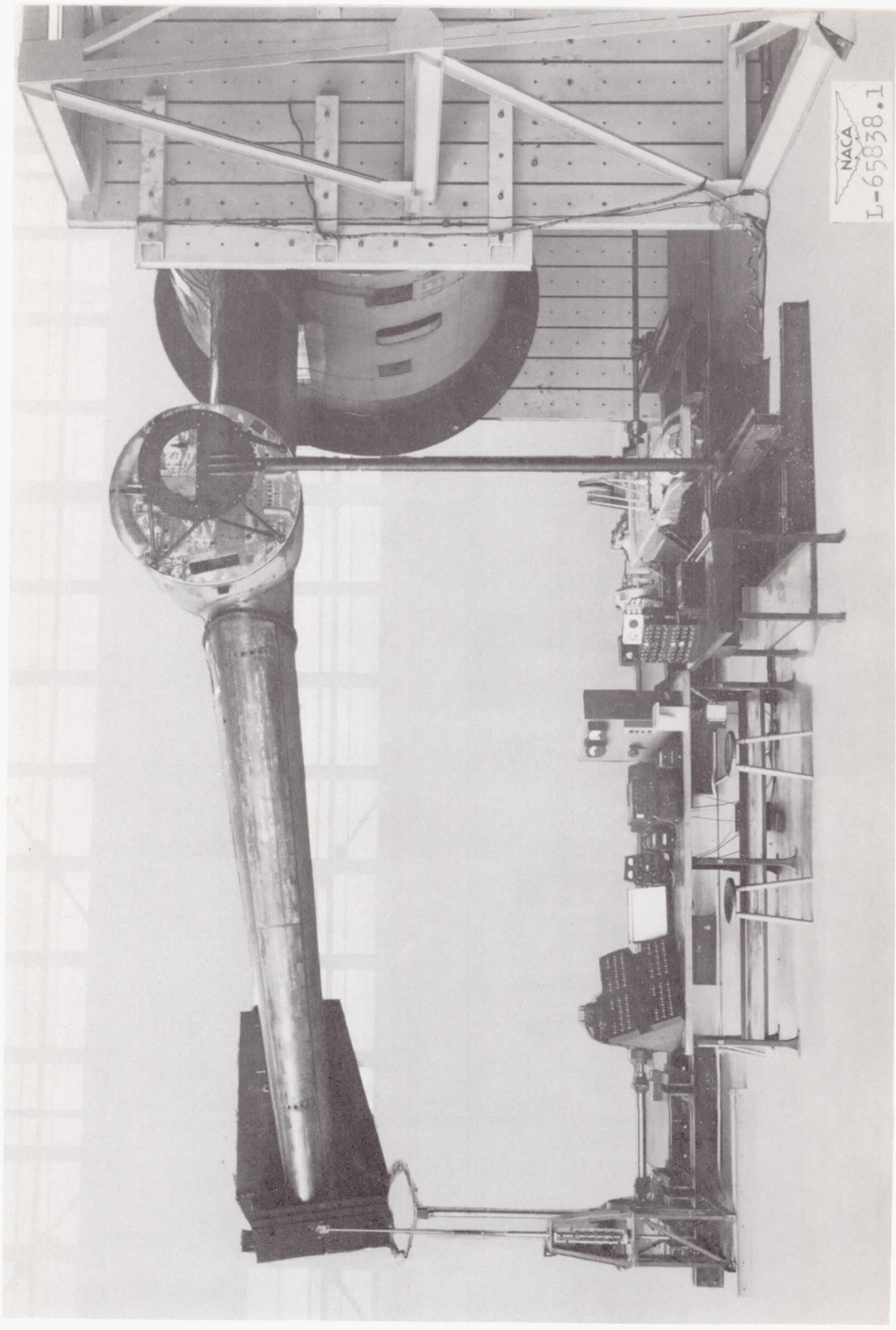

Figure 2.- General view of half of test setup.

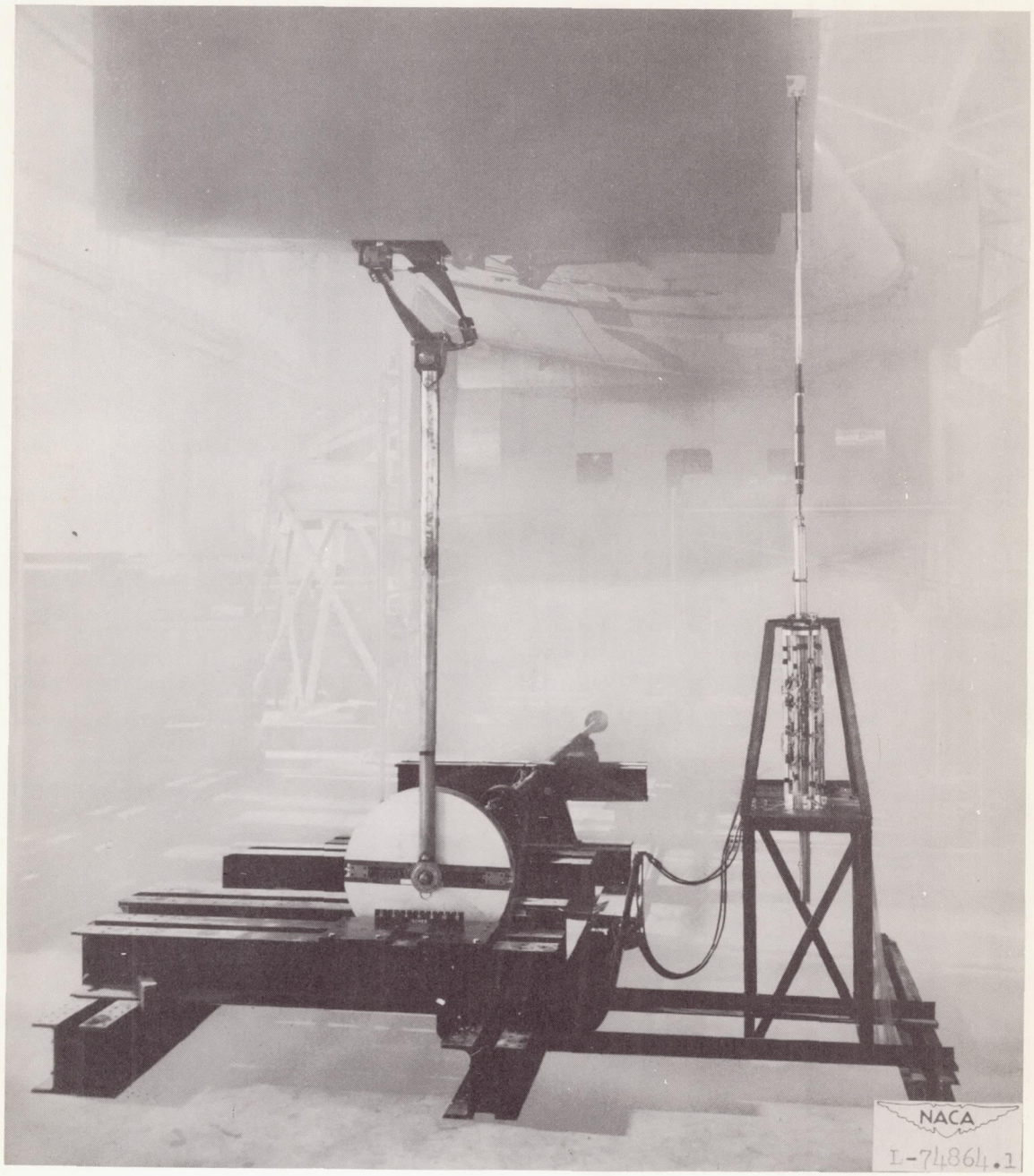

Figure 3.- Exciter spring system and amplitude-measuring microswitch assembly.

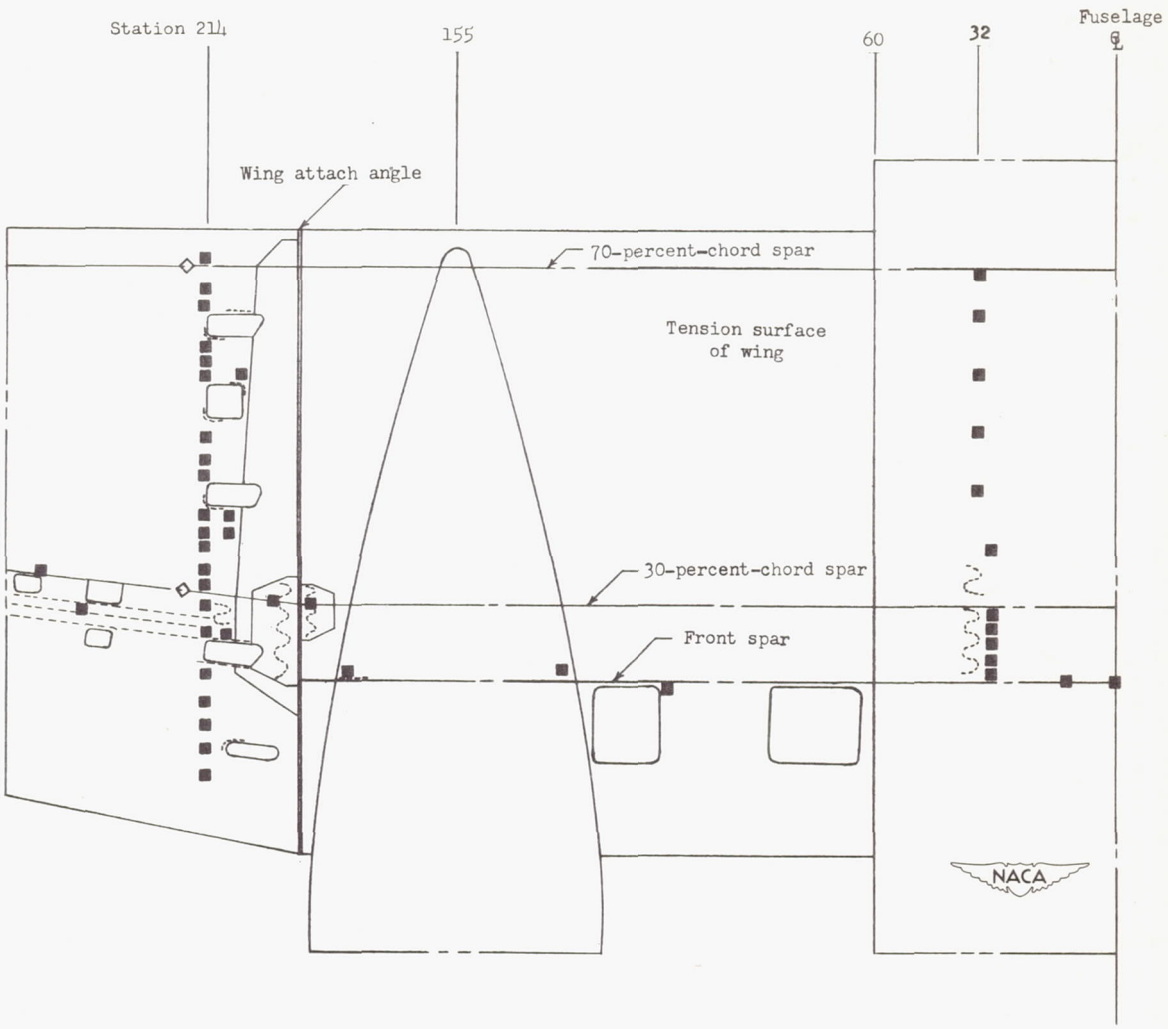

Figure 4.- Location of wing instrumentation. Installations are the same on the other wing.

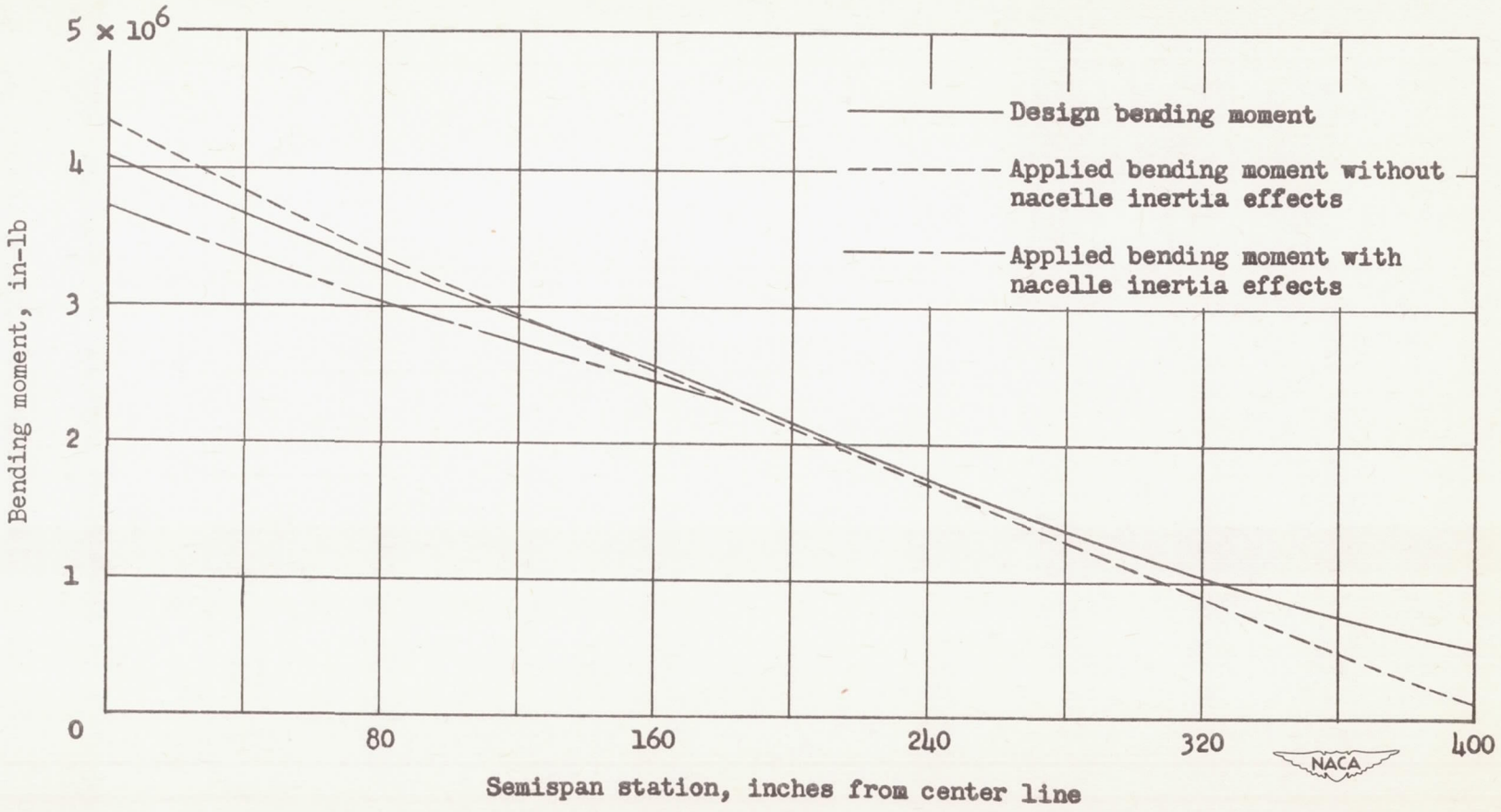

Figure 5.- Comparison of design and applied bending moment for the 1 g level-flight condition.

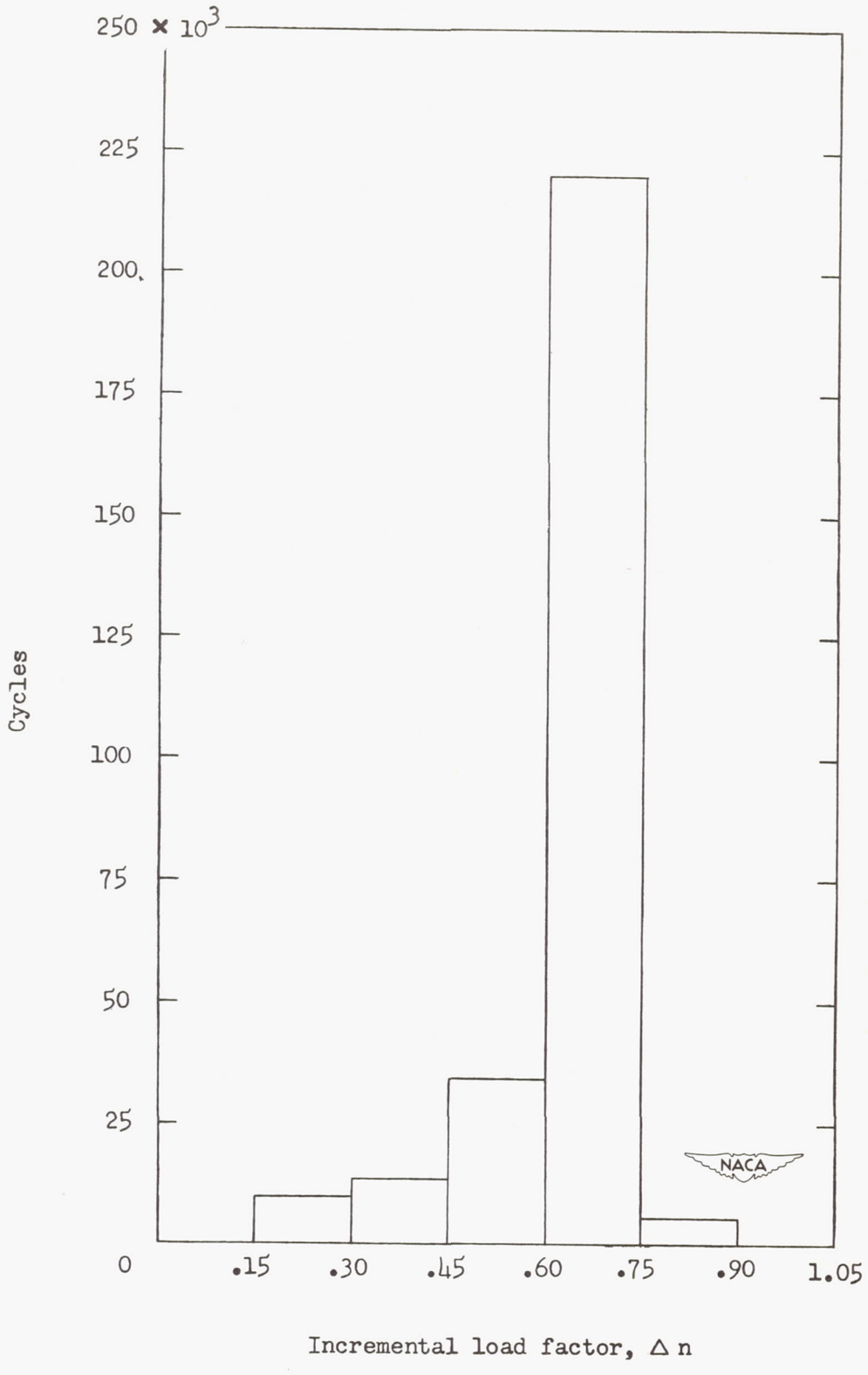

Figure 6.- Frequency distribution of applied loads.

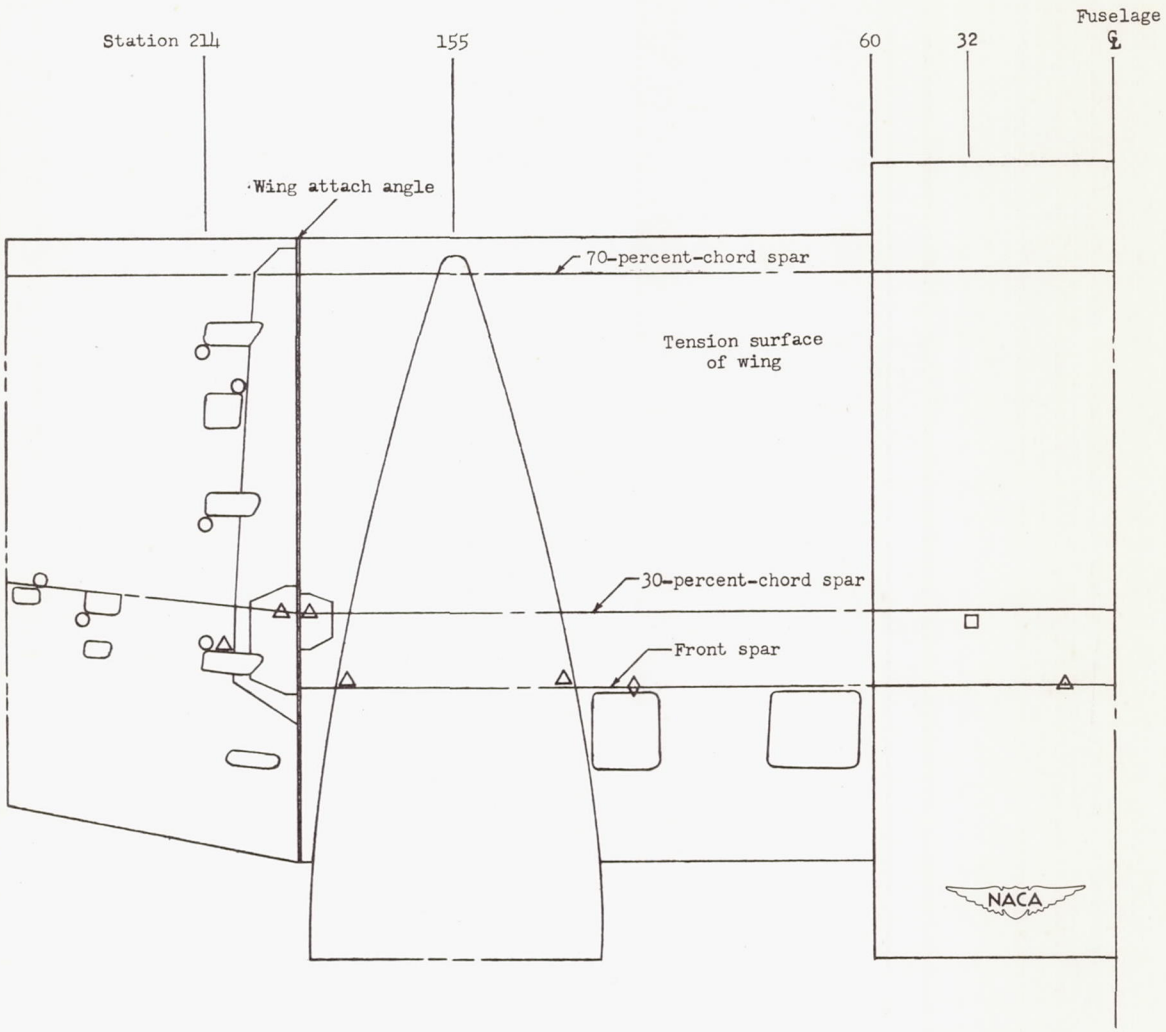

○	Type I	Failures originating at the corners of inspection cutouts
□	Type II	Failures originating in riveted tension joints
◊	Type III	Failures originating in riveted shear joints
△	Type IV	Failures originating in section at geometrical discontinuities

Figure 7.- Location and types of fatigue failures.

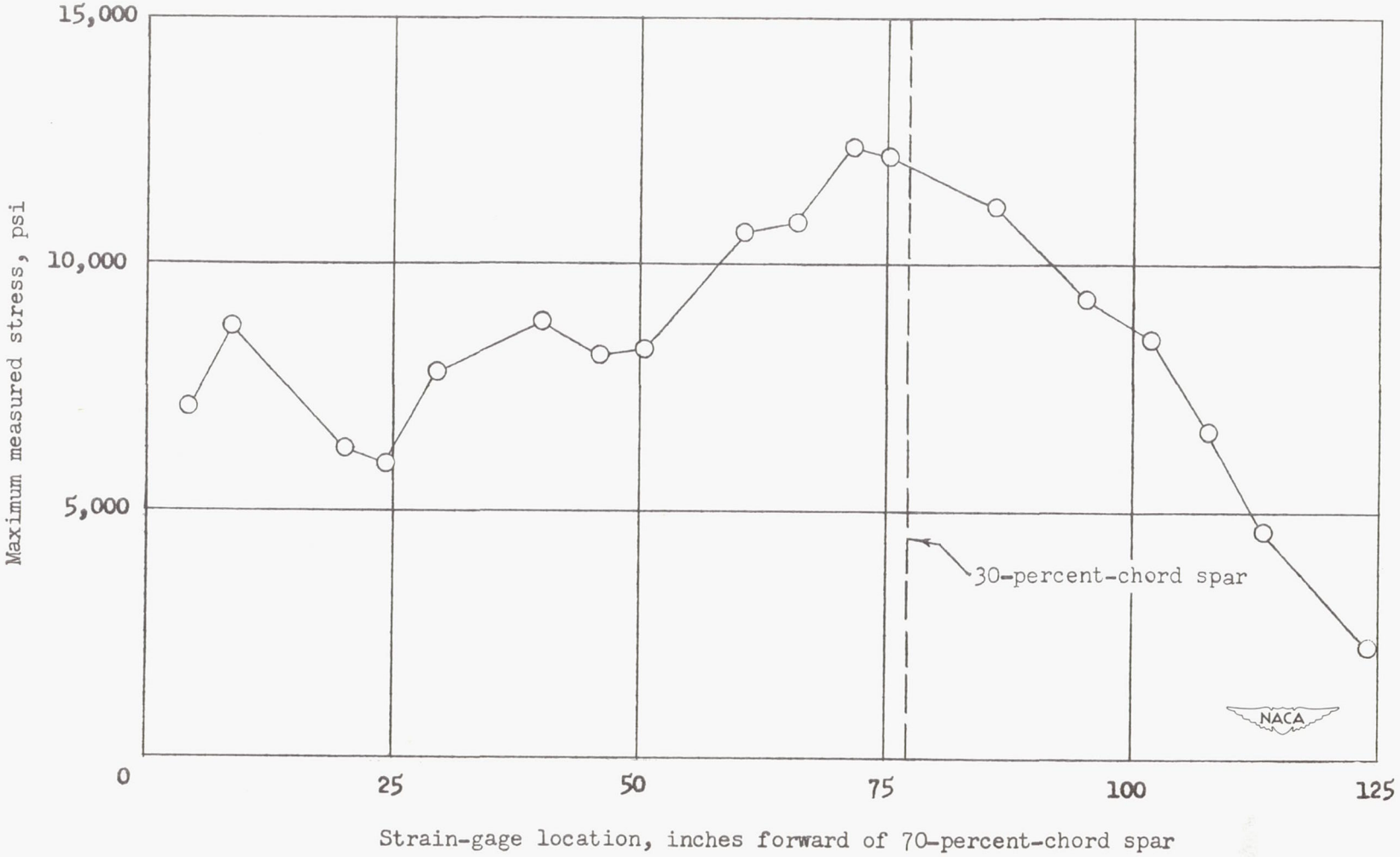

Figure 8.- Chordwise distribution of 1.625g measured stress at station 214.

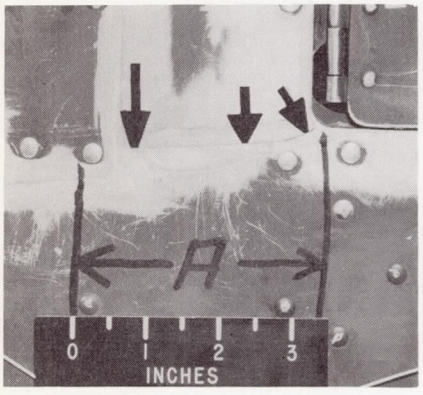

(a) Start of failure.

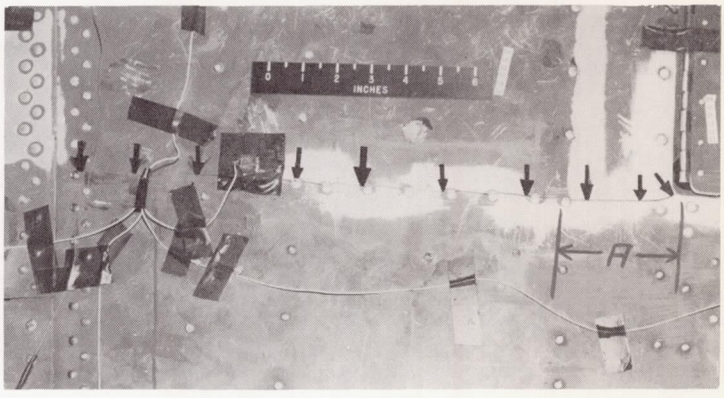

(b) Intermediate stage of failure.

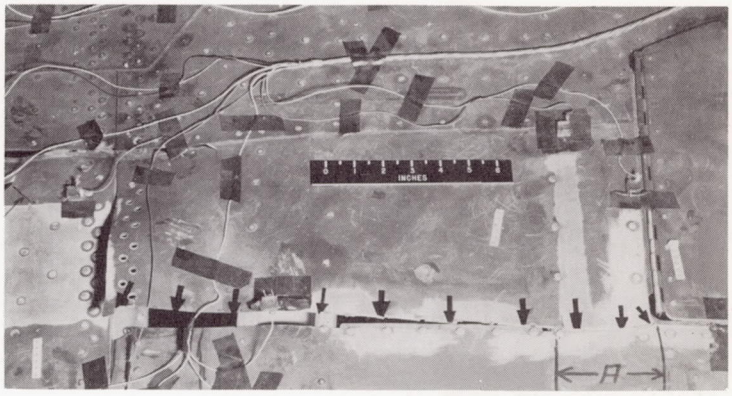

(c) Final stage showing failure of 30-percent-chord spar. NACA L-77922

Figure 9.- Three stages of typical failure that originated at corner of inspection cutout.

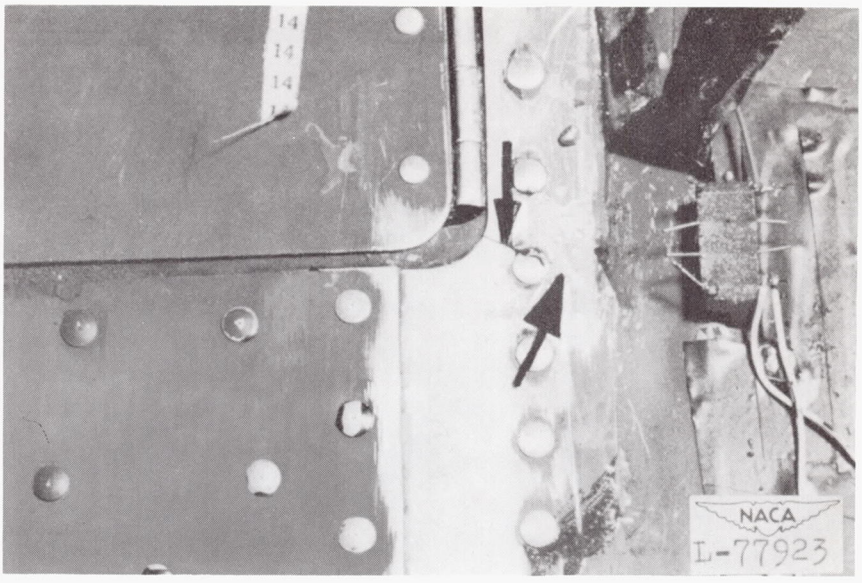

Figure 10.- Typical example of consistent failure that originated at corner of inspection cutout.

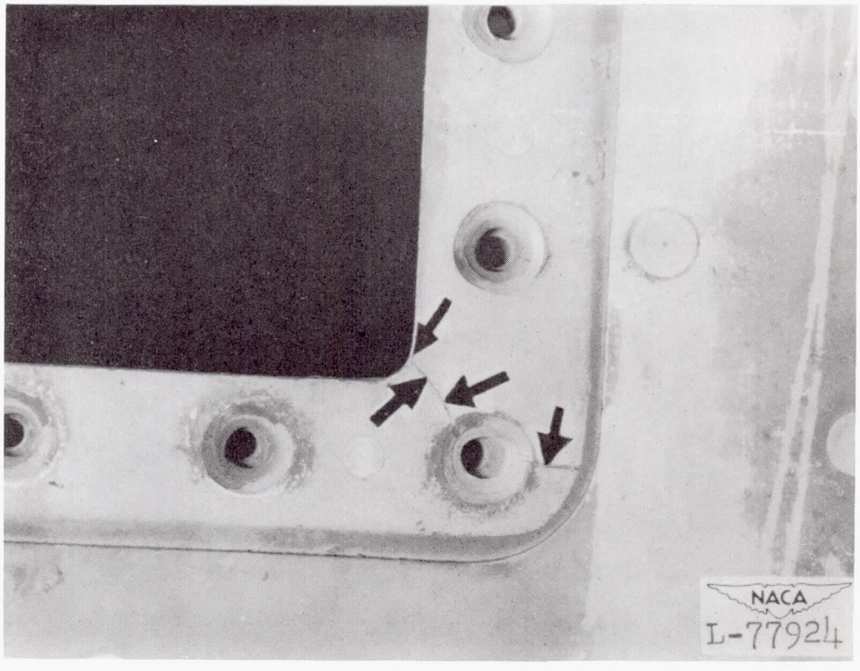

Figure 11.- Failure that originated in sharp corner radius of an internal reinforcing doubler plate.

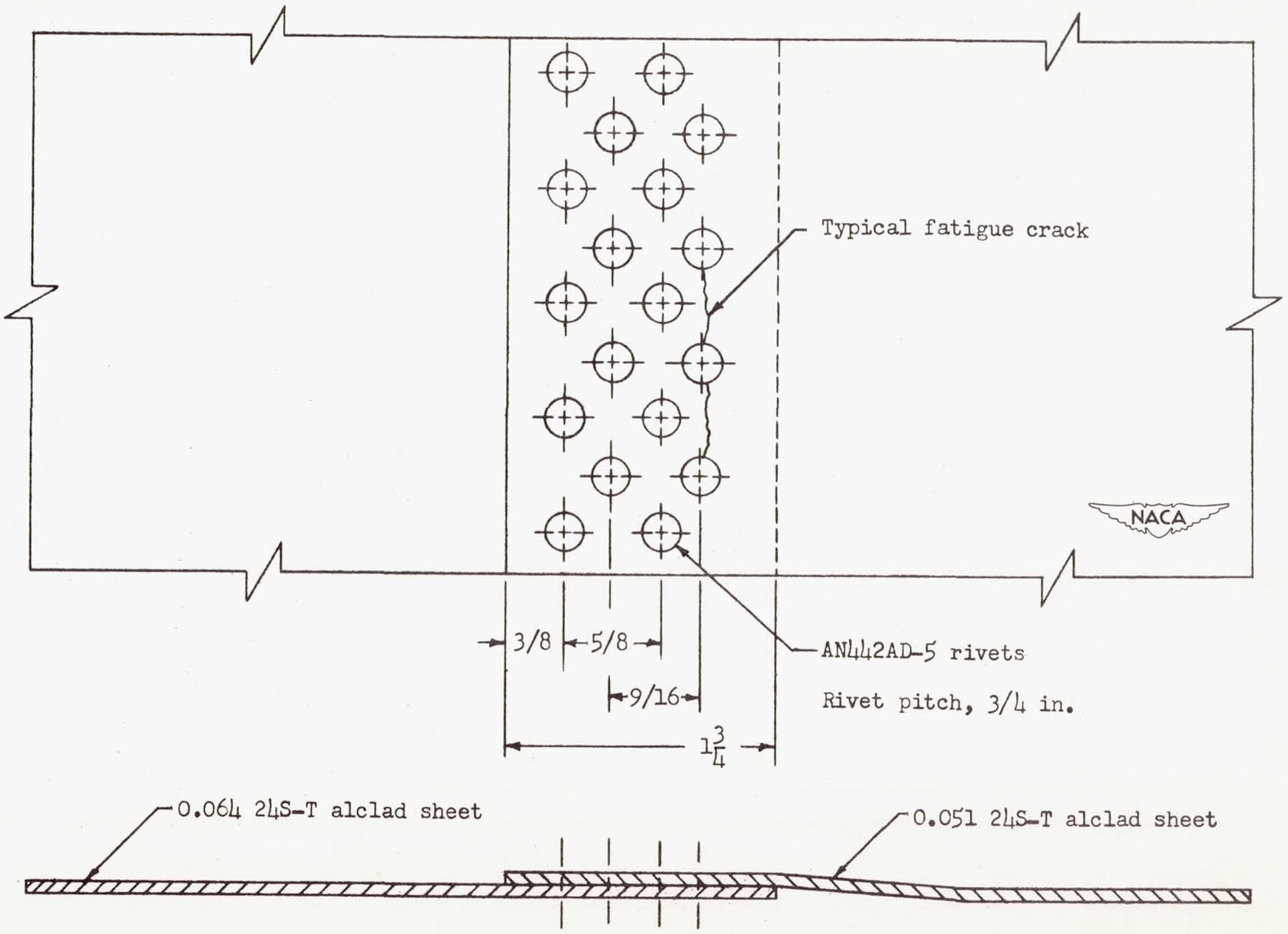

Figure 12.- Details of riveted tension joint at span station 32. All dimensions are in inches.

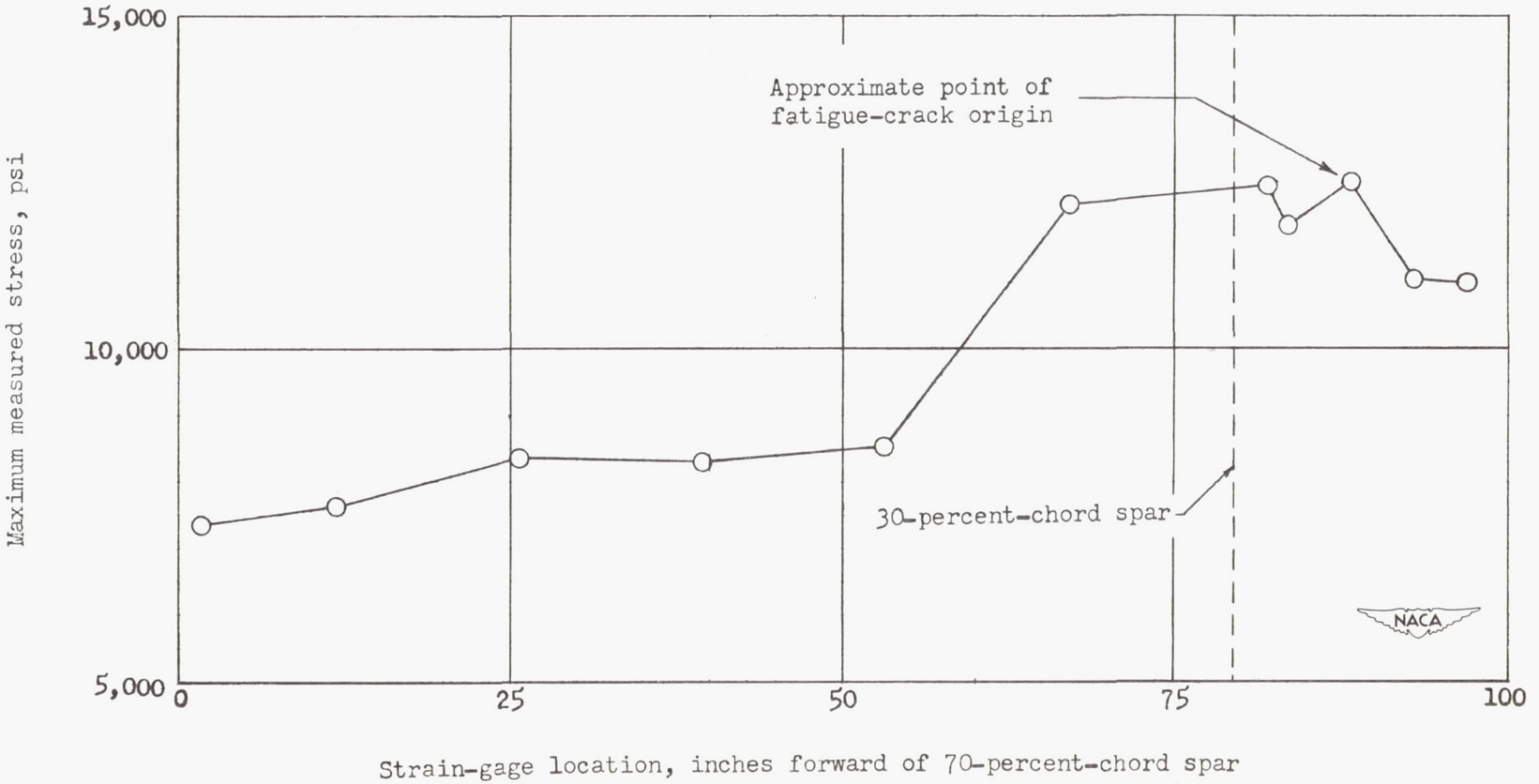

Figure 13.- Chordwise distribution of 1.625g measured stress at station 32.

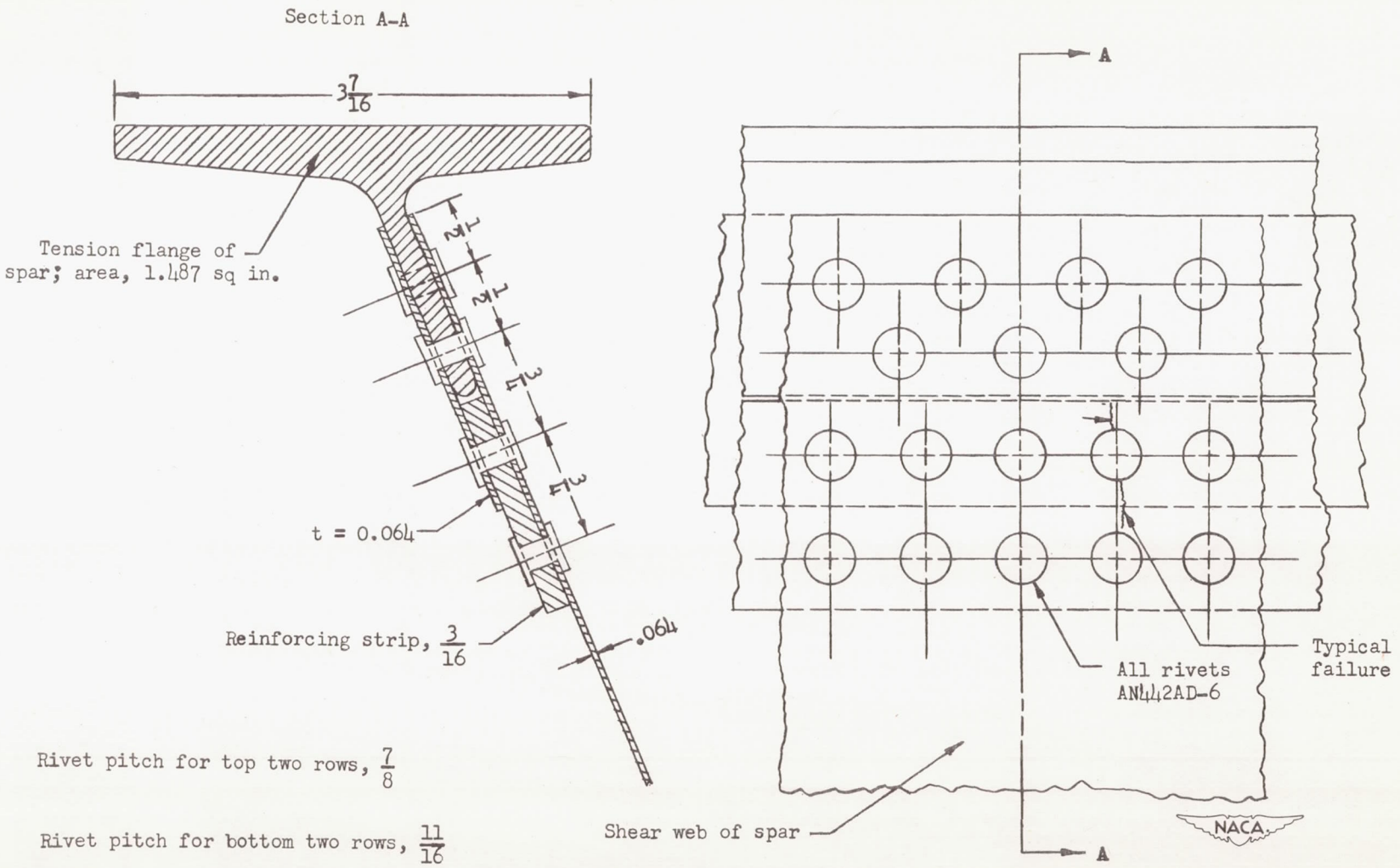

Figure 14.- Details of riveted shear joint at span station 120. All dimensions are in inches.

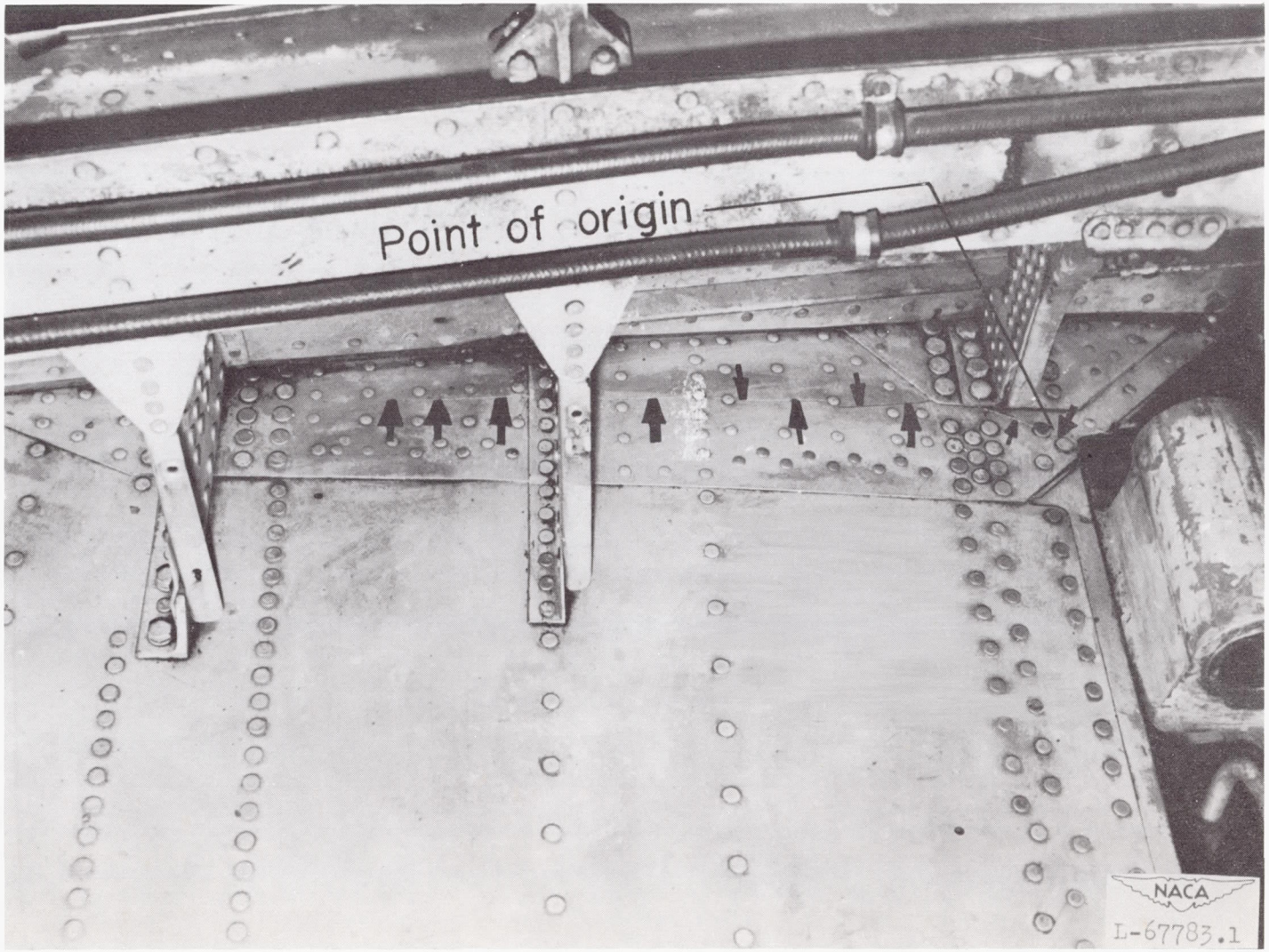

Figure 15.- Failure inside right nacelle, span station 170.

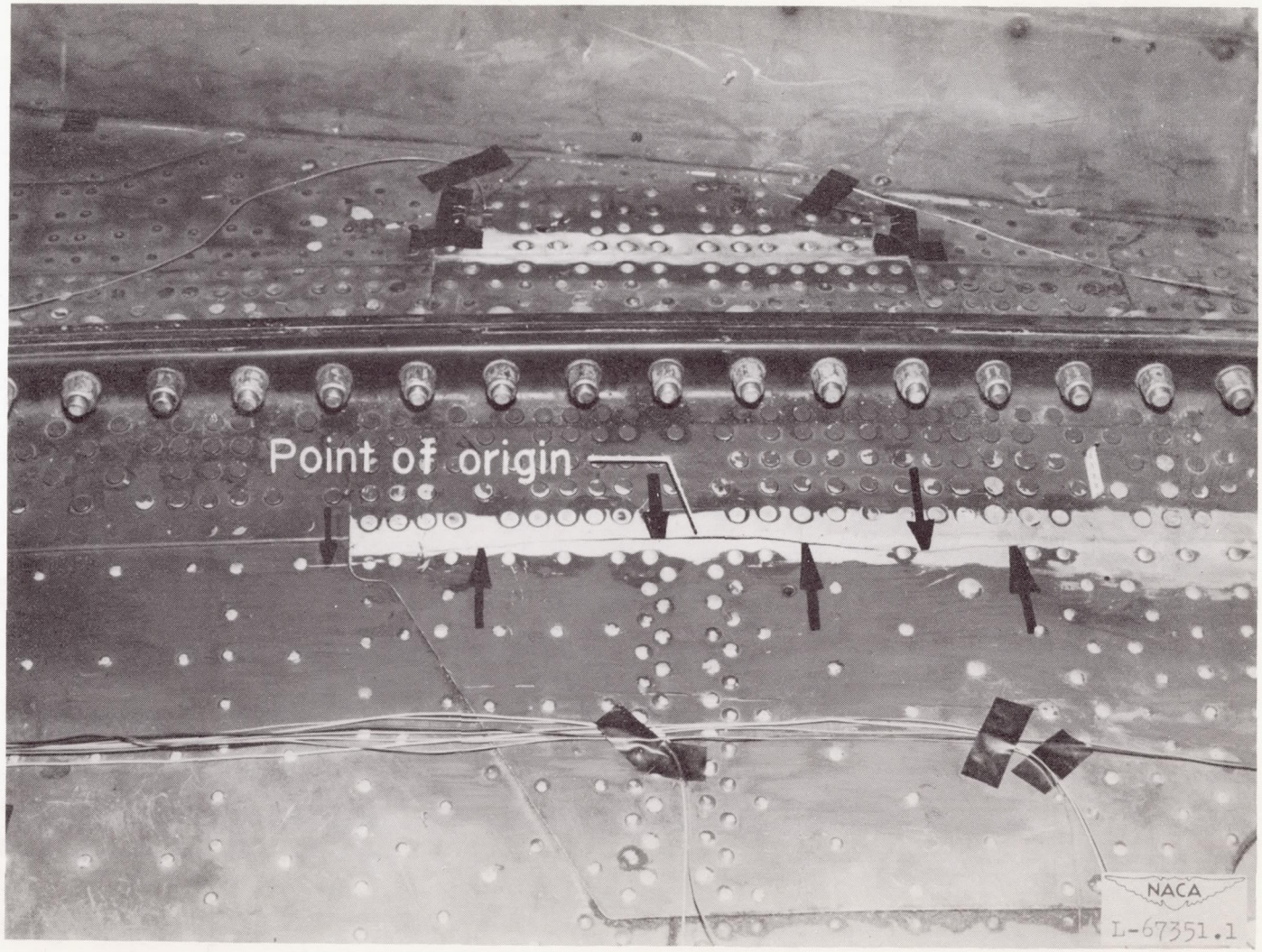

Figure 16.- Failure that initiated in a joggle of an external reinforcing doubler plate.

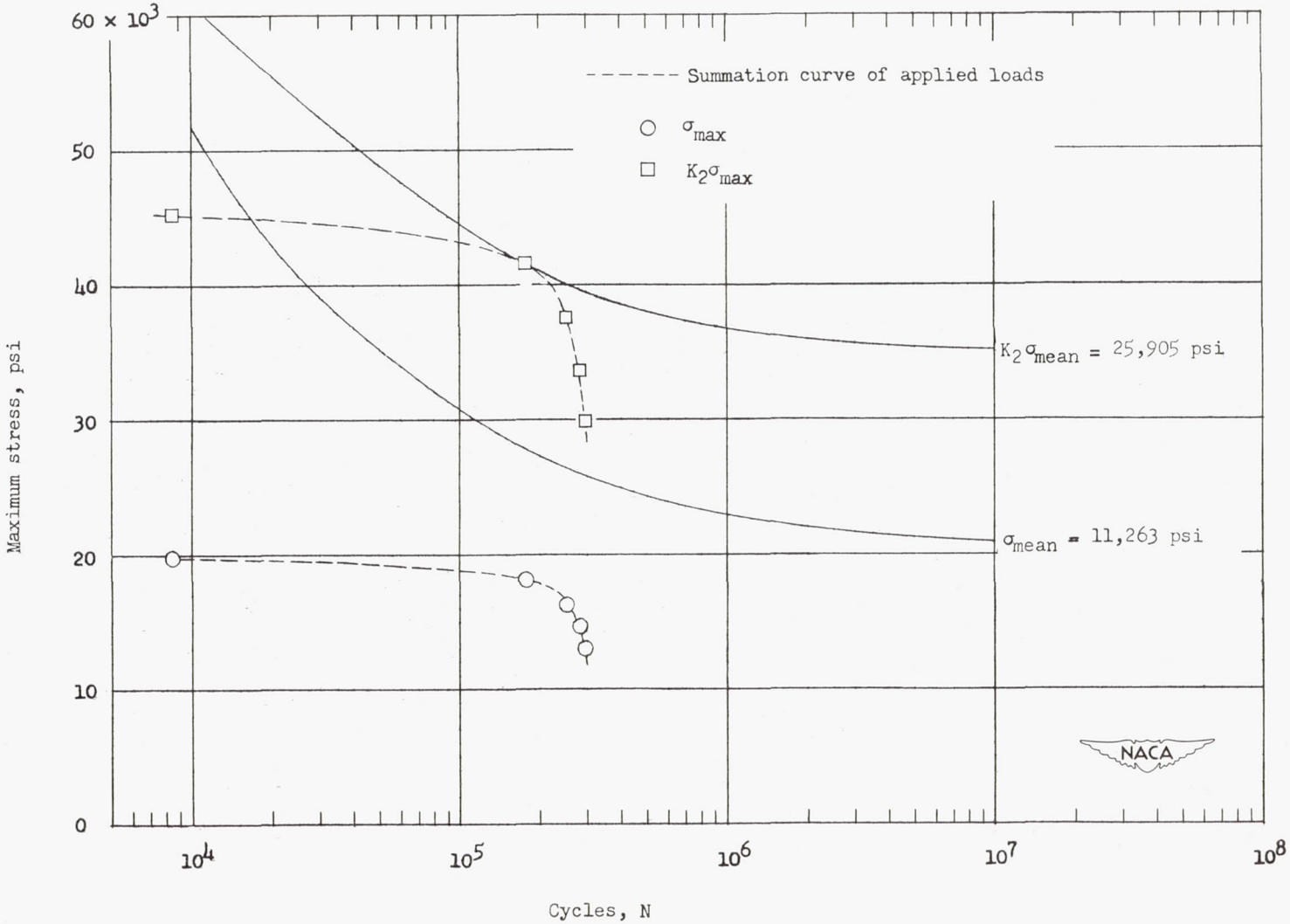

Figure 17.- Typical expansion of summation curves for determination of effective stress concentration factor K_2.

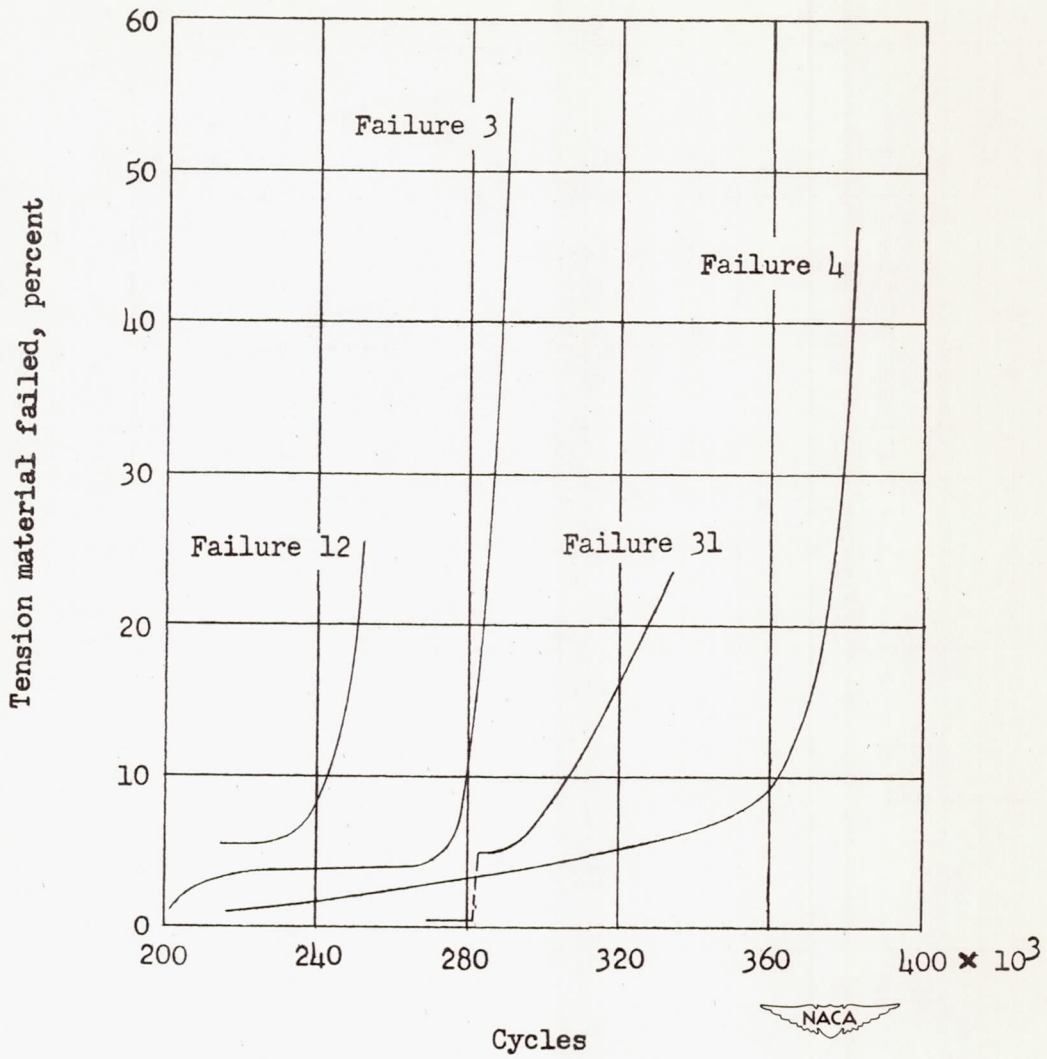

Figure 18.- Crack growth of several fatigue failures.

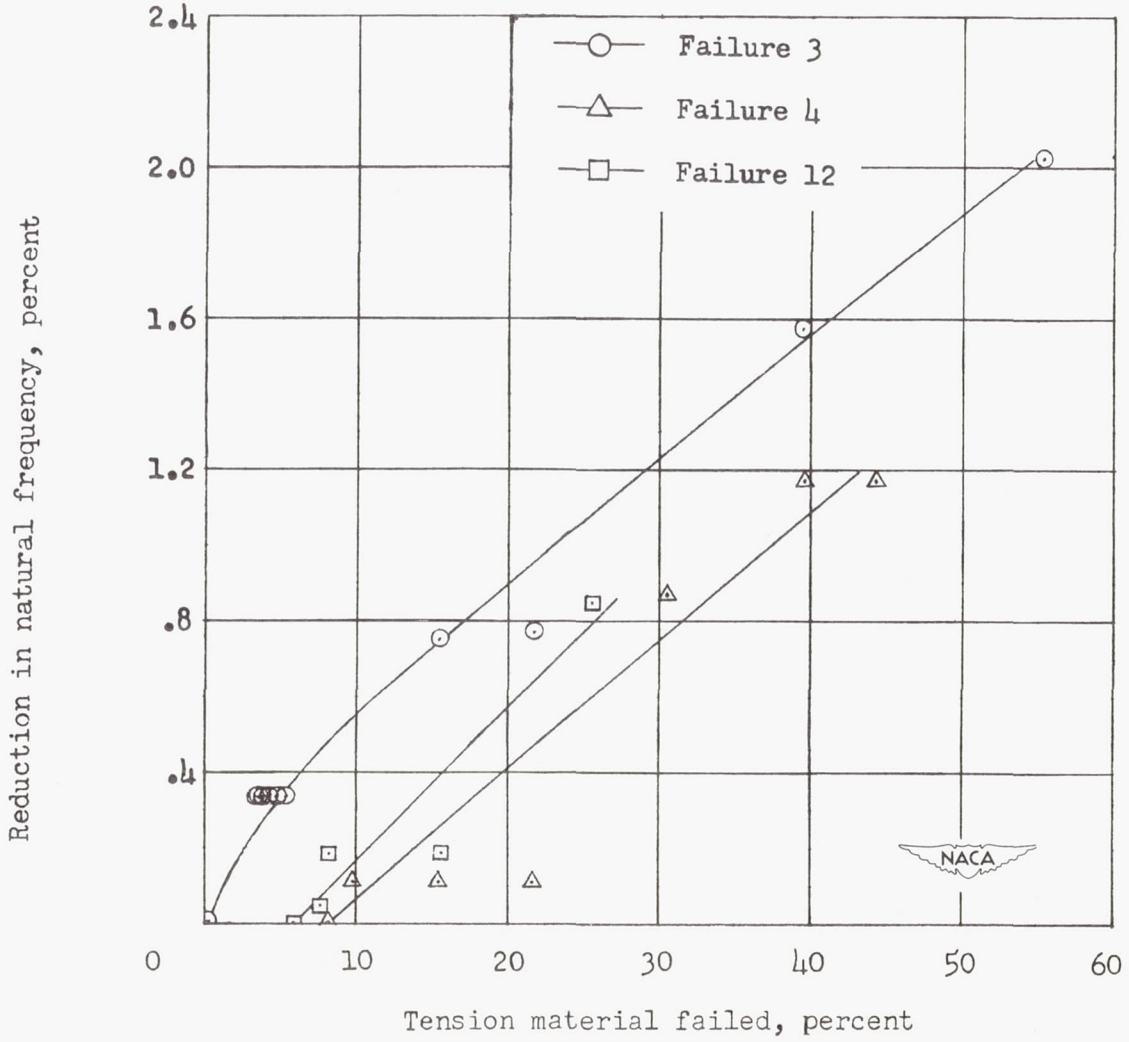

Figure 19.- Variation of natural frequency of test specimen with loss of tension material.

NACA-Langley - 4-6-53 - 1000